

Impact of control measures and typhoon weather on characteristics and formation of PM_{2.5} during the 2016 G20 summit in China

Yanru Zhang^{a,b,c}, Zhenyu Hong^{a,b,c}, Jinsheng Chen^{a,b,*}, Lingling Xu^{a,b,**}, Youwei Hong^{a,b}, Mengren Li^{a,b}, Hongfei Hao^d, Yanting Chen^{a,b}, Yuqing Qiu^{a,b,c}, Xin Wu^{a,b,c}, Jian-Rong Li^{a,b}, Lei Tong^{a,b}, Hang Xiao^{a,b}

^a Center for Excellence in Regional Atmospheric Environment, Institute of Urban Environment, Chinese Academy of Sciences, Xiamen, 361021, China

^b Key Laboratory of Urban Environment and Health, Institute of Urban Environment, Chinese Academy of Sciences, Xiamen, 361021, China

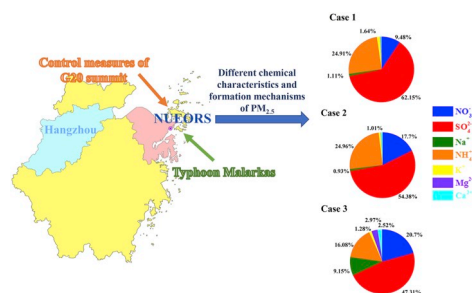
^c University of Chinese Academy of Sciences, Beijing, 100086, China

^d LAPC, Institute of Atmospheric Physics, Chinese Academy of Sciences, Beijing, 100029, China

HIGHLIGHTS

- Hourly PM_{2.5}, WSII, and BC were measured under control measures and typhoon.
- High PM_{2.5} under control measures due to stagnant weather and transport.
- Stagnant weather with high RH was beneficial for formation of SO₂ to sulphate.
- Sea salt brought by typhoon favored nitrate formation even under low NO₂.

GRAPHICAL ABSTRACT



ARTICLE INFO

Keywords:

Secondary inorganic aerosol
G20
Control measures
Typhoon
Regional transport
Formation mechanism

ABSTRACT

The implementation of strict emission control during the G20 summit in China and the occurrence of Typhoon Malarkas in September 2016 provided a valuable opportunity to examine the role of control measures and special weather condition in the formation of PM_{2.5}. Water-soluble inorganic ions (WSII) were measured hourly in addition to PM_{2.5} mass concentration and black carbon (BC) and gaseous pollutants in Ningbo located in the Yangtze River Delta (YRD) region of China. Three distinct cases, i.e., a control case, a normal case, and a typhoon case, were investigated during the study period. PM_{2.5} was higher in the control case (37.5 μg m⁻³) than in the normal case (29.8 μg m⁻³), whereas the lowest PM_{2.5} (14.2 μg m⁻³) was observed in the typhoon case. The analyses of meteorology and backward trajectory suggested that stable weather and regional transport from inland regions accounted for the high PM_{2.5} under strict control. Only the concentrations of Ca²⁺ and NO₃⁻ decreased in the control case, while those of all water-soluble inorganic components (except Na⁺ and Mg²⁺) decreased substantially in the typhoon case. SO₄²⁻ dominated the WSII, with the highest contribution, 62%, in the control case. This result was attributed to a stagnant atmosphere with a high relative humidity (RH), which was

* Corresponding author. Center for Excellence in Regional Atmospheric Environment, Institute of Urban Environment, Chinese Academy of Sciences, Xiamen, 361021, China.

** Corresponding author. Center for Excellence in Regional Atmospheric Environment, Institute of Urban Environment, Chinese Academy of Sciences, Xiamen, 361021, China.

E-mail addresses: jschen@iue.ac.cn (J. Chen), linglingxu@iue.ac.cn (L. Xu).

<https://doi.org/10.1016/j.atmosenv.2020.117312>

Received 31 May 2019; Received in revised form 20 January 2020; Accepted 25 January 2020

Available online 5 February 2020

1352-2310/© 2020 Elsevier Ltd. All rights reserved.

beneficial for the transformation of SO_2 to SO_4^{2-} . The control and typhoon cases both resulted in extremely low NO_2 , but the contribution of NO_3^- to $\text{PM}_{2.5}$ was reduced in the control case and increased in the typhoon case. The close correlation of the NOR (nitrate oxidation ratio) with Na^+ and Mg^{2+} in the typhoon case was indicative of sea salt associated with the typhoon which provided a surface for the heterogeneous formation of NO_3^- . The presented results facilitate a better understanding of the characteristics and formation of $\text{PM}_{2.5}$ under the influence of artificial control and natural intervention.

1. Introduction

Atmospheric $\text{PM}_{2.5}$ (particulate matter with a dynamic equivalent diameter less than $2.5 \mu\text{m}$) pollution is influenced by many factors. Fine particles can be directly released into the atmosphere by anthropogenic and natural activities. They can be subsequently transformed from primary pollutants (such as sulphur dioxide (SO_2) and nitrogen oxides (NO_x)) (Gard et al., 1998; George et al., 2015; Zhang et al., 2015). Huang et al. (2012) presented three typical kinds of air pollution in Shanghai: secondary pollution episode, dust pollution episode, and biomass combustion pollution episode with $\text{PM}_{2.5}$ dominated by secondary aerosols, minerals, and K^+ and carbonaceous aerosol, respectively. Fu et al. (2008) and Wang et al. (2006) determined that the heterogeneous reactions from SO_2 and NO_2 to SO_4^{2-} and NO_3^- plays an important role in the formation of $\text{PM}_{2.5}$. Except for the chemical factors, previous studies have also reported on the conducive effects of regional transport, relative humidity (RH), and stagnant meteorological conditions on the formation of $\text{PM}_{2.5}$ (Wang et al., 2018; Li et al., 2017b). Overall, the formation mechanism of $\text{PM}_{2.5}$ in the atmosphere is related to the emission sources, meteorological conditions, and transport of pollutants (Sun et al., 2006; Fu et al., 2008; Huang et al., 2012; Li et al., 2015; Zhang et al., 2015; Hua et al., 2016; Han et al., 2016a).

China is still under tremendous threat of $\text{PM}_{2.5}$ pollution (Huang et al., 2012; Ming et al., 2017). The Chinese government has implemented the "Atmospheric Pollution Prevention and Control Action" in recent years with the aim of relieving air pollution in China. Moreover, the effects of the control measures on the reduction of pollution have been obvious during major events such as the Beijing 2008 Olympic Games, the 2014 Asia-Pacific Economic Cooperation (APEC) summit, and the China Victory Day Parade (V-Day Parade) in 2015 (Sun et al., 2016; Xu et al., 2017; Liang et al., 2017). A series studies have been conducted on the major species (element, water-soluble ions, and BC) of PM during the 2008 Olympic Games, and the results showed that the emission mitigation measures had successful reduction for the pollutants (Schleicher et al., 2011, 2012; Li et al., 2012). The obvious reduction of $\text{PM}_{2.5}$ composition also found under the strict emission control of the V-Day Parade in 2015 comparing to the same period of a few years earlier (Han et al., 2016b). Although the emission restriction policy resulted in the suppression of PM, some secondary pollution episodes formed via the photochemical reaction and regional transport still could happen. In the early control period of the Olympic Games, a vehicle emissions and coal combustion were achieved, but the formation of secondary aerosol in regional scales still increased (Sun et al., 2011, 2016; Wang et al., 2010).

As for the possibilities of the pollution episodes even under the emission control period, it is important to understand the formation mechanism of $\text{PM}_{2.5}$ to better regulate air quality. However, some special weather conditions also have a significant impact on the formation and mitigation of pollutants (Yan et al., 2016; Wang et al., 2005a). For example, typhoons are the predominant weather conditions during the summer monsoon season in East Asian. Fang et al. (2009) determined that typhoons re-suspended dust and caused an increase of particles (Fang et al., 2009). Meanwhile, the special meteorological conditions caused by a typhoon such as heavy rainfall and active atmospheric movement, could decrease atmospheric pollutants and affect the formation mechanism of $\text{PM}_{2.5}$ (Yan et al., 2016; Fang et al., 2009). Control measures and typhoon both significantly reduce the concentration of

atmospheric primary pollutants. Nevertheless, there are few comparative studies on the roles they play in the formation mechanism of $\text{PM}_{2.5}$.

The 2016 G20 summit was held on 4–5 September 2016 at Hangzhou, the Yangtze River Delta (YRD) region of China. To improve air quality, control measures such as the closure of industrial plants with high emission, cessation of construction activities, and the restriction of traffic flow, were adopted by the government in the YRD region from the middle of August until the summit ended. According to the distance from the main stadium, the YRD region was divided into core control zone, strict control zone, and normal control zone. The adjacent provinces (such as Shanghai, Jiangsu, Anhui) also implemented some mitigation measures to ensure the air quality. Ningbo, as a city adjoined Hangzhou, was part of the strict control zone. During the G20 summit, the government reduced the emission of pollutants by controlling or prohibiting industrial, construction, and traffic activity in the YRD region. After the G20 summit, it was determined that typhoon Malarks had a significant influence on the YRD region, especially the coastal cities in the YRD region. Therefore, the strict control measures and typhoon occurred within a short period (September 2016) and offers a valuable opportunity to study the difference in the formation mechanism of $\text{PM}_{2.5}$. Several studies have reported the air quality in Hangzhou under the emission control of the 2016 G20 summit. Li et al., (2017c) had found the high reduction of particulate matter in Hangzhou during the control period of G20 summit compared to the period previous to the G20 summit. Li et al., (2017d) found the night time transport of pollutants was unfavourable for the mitigation of pollutants in Hangzhou even under the strict emission control of the G20 summit. However, few studies were focused on the comparison of different formation mechanism of secondary inorganic aerosols influenced by the control measures and the typhoon weather. This study aims to: (1) differentiate between the characteristics of $\text{PM}_{2.5}$ and the gaseous pollutants that are affected by the control measures and typhoon weather; (2) elucidate the influence of meteorological conditions on the water-soluble inorganic components of $\text{PM}_{2.5}$; (3) investigate the formation mechanism of secondary inorganic aerosols under control measures and typhoon weather.

2. Methods

2.1. Field observation

2.1.1. Description of the sampling site

The observations campaign was conducted on the rooftop of the Ningbo Urban Environment Observation and Research Station (NUEORS) building (29.87°N , 121.91°E , 10 m a.s.l), located in the Beilun District of Ningbo in the YRD region, China (Fig. 1). NUEORS is a suburban site that is 20 m away from the coastline and approximately 172 km northwest from the host city of the 2016 G20 summit. Southeast of the sampling site is a park, northeast is a residential area, while in the southwest and northwest are industrial parks.

2.1.2. Continuous observations of $\text{PM}_{2.5}$ and meteorological parameters

Intensive field observations of atmospheric pollutants were conducted during 1–20 September 2016. The mass concentration of $\text{PM}_{2.5}$ was determined using the method of tapered element oscillating microbalance with a continuous particulate monitor (TEOM 1405-D, Thermo Co., USA) at 1-h resolution. CO , ozone (O_3), SO_2 , and NO_x were measured using a gas analyser (48i, 49i, 43i, 42i, Thermo Fisher

Scientific, Waltham, MA, USA). Automatic recording of meteorological parameters including ambient temperature (T), pressure (P), wind direction (WD), wind speed (WS), and relative humidity (RH) was simultaneously performed automatically by the weather station (MAWS301, Vaisala, Finland) at NUEORS.

The concentration of the water-soluble inorganic ions (WSII, including Cl^- , NO_3^- , SO_4^{2-} , Na^+ , NH_4^+ , K^+ , Ca^{2+} , and Mg^{2+}) of $\text{PM}_{2.5}$ at 1-h resolution was measured using an online monitor for Aerosols and Gases (MARGA, Metrohm Co., Switzerland) and the flow rate was 16.7 L min^{-1} . The WSII in $\text{PM}_{2.5}$ was acquired using a stem jet aerosol collector and was analysed via ion chromatography after dissolving in Milli-Q pure water containing 10 mg L^{-1} peroxide (H_2O_2). The eluent for cation analysis was 3.2 mmol L^{-1} nitric acid (HNO_3), and 7.0 mmol L^{-1} sodium carbonate monohydrate ($\text{Na}_2\text{CO}_3 \cdot \text{H}_2\text{O}$) and 8.0 mmol L^{-1} sodium bicarbonate (NaHCO_3) for the anion. Solution of Lithium bromide (LiBr) was used hourly as internal standard liquid to calibrate the instrument. The detection limits of Na^+ , NH_4^+ , K^+ , Ca^{2+} , Mg^{2+} , NO_3^- , SO_4^{2-} , and Cl^- were 0.05, 0.05, 0.09, 0.09, 0.06, 0.05, 0.04, and $0.01 \mu\text{g m}^{-3}$, respectively. The precision of all ion's concentrations was $0.001 \mu\text{g m}^{-3}$ and it was reported the collection efficiency can achieve 99% (Cowen et al., 2012). However, the data quality of Cl^- was poor due to instrumentation problems, and was excluded in this study.

Black carbon (BC) in $\text{PM}_{2.5}$ was measured using a model AE-31 Aethalometer (Magee Co., USA). The sampling flow was set to 4.0 L min^{-1} and the concentration of BC was monitored every 5 min at seven wavelengths (370, 470, 520, 590, 660, 880, and 950 nm). In this study, we chose the concentration at $\lambda = 880 \text{ nm}$ as the BC concentration.

2.2. Backward trajectory analyses

Backward trajectory analysis was performed to explore the origins and the transport pathway of the air masses that arrived at NUEORS using the Hybrid Single Particle Lagrangian Integrated Trajectory model (HYSPPLIT) developed by NOAA ARL (Draxler et al., 1997; Stein et al., 2016). The meteorological dataset with a horizontal resolution of 1° longitude \times 1° latitude was acquired from the NCEP/GDAS. 48-h backward trajectory analysis was conducted at a ground elevation of 100 m every 6 h (0:00, 6:00, 12:00, 18:00, local time) at NUEORS. Clustering was then performed to group the calculated backward trajectories into different categories based on the total spatial variance (TSV).

2.3. Data analysis method

Sulphates and nitrates are usually associated with the transformation of SO_2 and NO_2 (Zhang et al., 2015; Li et al., 2017a). The sulphate oxidation ratio (SOR) and the nitrogen oxidation ratio (NOR) are conducive to the investigation of the conversion efficiencies of SO_2 to SO_4^{2-} and NO_2 to NO_3^- , respectively. SOR and NOR were calculated as follows:

$$\text{SOR} = \frac{[\text{SO}_4^{2-}]}{[\text{SO}_4^{2-}] + [\text{SO}_2]}, \quad (1)$$

$$\text{NOR} = \frac{[\text{NO}_3^-]}{[\text{NO}_3^-] + [\text{NO}_2]}, \quad (2)$$

where [x] denotes the molar concentration of the chemical species x.

3. Results

3.1. General characteristics of $\text{PM}_{2.5}$ and the gaseous pollutants

As shown in Fig. 2, the mean hourly concentration of $\text{PM}_{2.5}$ at NUEORS during the observation period was $23.6 \pm 12.0 \mu\text{g m}^{-3}$ with a range of 1.0–54.0 $\mu\text{g m}^{-3}$. The temporal distribution of the gaseous pollutants is similar to that of $\text{PM}_{2.5}$. Three cases were investigated during the observation period. Case 1 (0:00 1 September – 12:00 4 September) was influenced by the strict control measures implemented during the G20 summit. The emission reductions for industry, power plant, residential, and transport sources in Zhejiang province was up to 65%. The emission reduction in the YRD region except Zhejiang (Shanghai, Anhui, Jiangsu) was about 40%, which covered the industry and the power plant (Li et al., 2017d). The mean concentration of $\text{PM}_{2.5}$ was $37.5 \mu\text{g m}^{-3}$ in Case 1, which slightly exceeded the Chinese National Ambient Air Quality Standard of $\text{PM}_{2.5}$ (NAAQS, $35.0 \mu\text{g m}^{-3}$) and was 1.5 times that of the World Health Organization guideline for $\text{PM}_{2.5}$ (WHO, $25.0 \mu\text{g m}^{-3}$). Case 2 (12:00 6 September – 23:00 11 September) was for the condition of normal emission of pollutants with the control measures stopped after 6 September. However, the average concentration of $\text{PM}_{2.5}$ ($29.8 \mu\text{g m}^{-3}$) was slightly lower in Case 2 than in Case 1. Case 3 (0:00 15 September – 23:00 20 September) was under the influence of the movement of typhoon Malarks on the sea surface of the

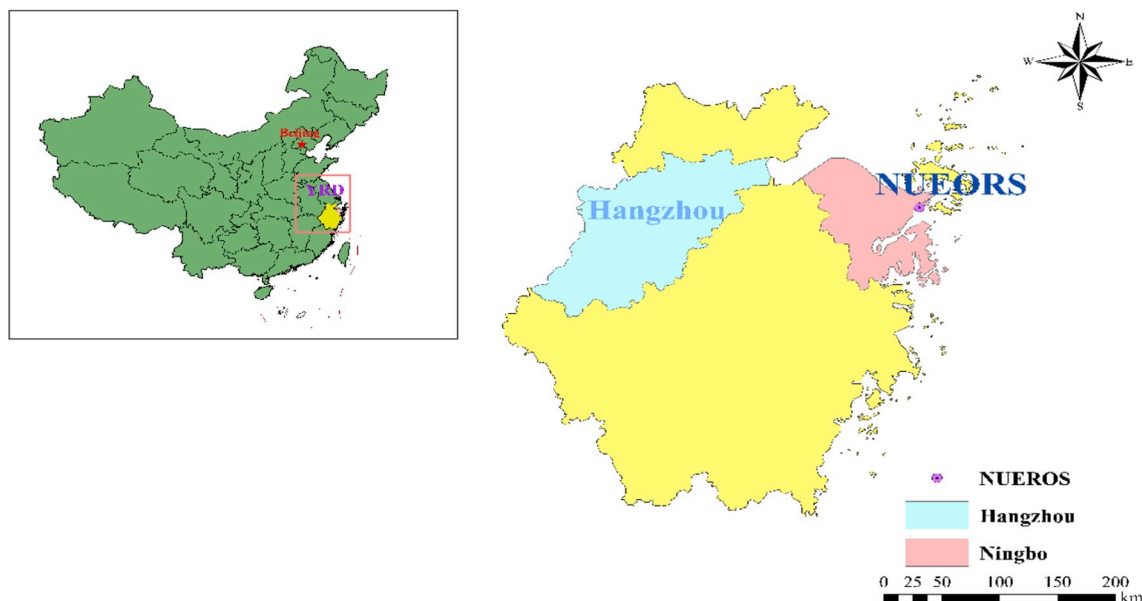


Fig. 1. The location of the Ningbo Urban Environment Observation and Research Station (NUEORS).

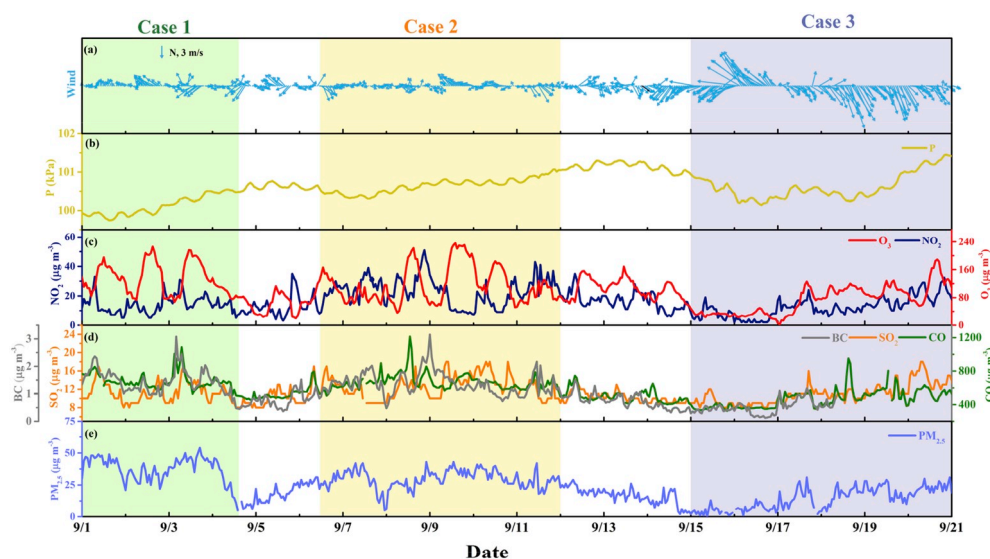


Fig. 2. Time series of (a) wind and (b) pressure (P); hourly concentrations of (c) O₃ and NO₂, (d) black carbon (BC), SO₂, and CO, (e) PM_{2.5}.

Pacific Ocean. The typhoon moved over the sea surface near Ningbo from southeast to northeast and finally landed in Japan on 20 September. The mean mass concentration (14.2 $\mu\text{g m}^{-3}$) of PM_{2.5} for Case 3 was the lowest among the three cases.

As presented in Fig. 2 and Table 1, the mean concentrations of SO₂ in Case 1 (11.3 $\mu\text{g m}^{-3}$) and Case 3 (10.9 $\mu\text{g m}^{-3}$) were comparable, while the value was slightly higher than for Case 2 (12.8 $\mu\text{g m}^{-3}$). Different from SO₂, the concentration of NO₂ varied dramatically. The NO₂ concentration increased to 22.9 $\mu\text{g m}^{-3}$ for Case 2, which was approximately twice that of Case 1 (14.2 $\mu\text{g m}^{-3}$) and Case 3 (12.3 $\mu\text{g m}^{-3}$). A lower NO₂ in Case 1 reflects the significant effect of the control measures on the traffic during the G20 summit. Strong wind and rainy weather due to the typhoon in Case 3 not only offered a favourable condition for the diffusion of NO₂ but also limited the traffic activities to a certain extent. Traffic control reduced NO emission and lowered the efficiency of O₃ destruction (oxidation of NO to form NO₂), which accounts for the highest concentration of O₃ in Case 1. Concentrations of CO in Case 1 and Case 2 was higher than in Case 3. BC as one of the major components

of PM_{2.5}, comprising 5.2% in PM_{2.5}. Average concentration of BC was highest in Case 1 (1.45 $\mu\text{g m}^{-3}$) followed by Case 2 (1.39 $\mu\text{g m}^{-3}$) and Case 3 (0.51 $\mu\text{g m}^{-3}$). Thus, the disadvantageous effect of air mass transport and atmospheric diffusion during the control period could be reasonably proposed for the higher concentration of primary pollutants CO and BC in Case 1. In summary, all the atmospheric pollutants (PM_{2.5}, PM₁₀, SO₂, NO₂, O₃, CO, and BC) decreased (by 14.2%–63.3%) during the typhoon case, whereas only SO₂ and NO₂ clearly decreased (by 11.5% and 38.1%) during the control case.

3.2. Atmospheric transport and diffusion condition

3.2.1. Backward trajectory analysis

To better understand the influence of regional transport on Ningbo for the different cases, backward trajectory analysis was performed and two clustering trajectories were obtained for each case (Fig. S1). In Case 1, one air mass trajectory represented short-range terrestrial transport (73.3%) and the other originated from the Yellow sea (26.7%). In Case 2, both trajectories were transported on the surface of the Yellow Sea. The two trajectories in Case 3 are attributed to the Yellow Sea (70.8%) and the East China Sea (29.2%), respectively. Comparing the backward trajectories of the three cases, Case 1 was more heavily influenced by the regional transport over land than Case 2 and Case 3. This partially accounts for the highest PM_{2.5} concentration in Case 1, even under the strict measure controls. Although the air masses in Case 2 and Case 3 were all transported over sea, the air mass in Case 2 originated from offshore sea (cluster 2, Fig. S1b) compared to the air mass in Case 3. This difference, to a certain extent, results in a higher PM_{2.5} concentration for Case 2 than in Case 3.

3.2.2. Meteorological conditions

The meteorological conditions also had considerable influence on the concentration of PM_{2.5}. As depicted in Figs. 2 and 5 and Table 1, the meteorological condition, especially WS, was distinctly different for the three cases. The average wind speed (5.2 m s^{-1}) for Case 3 was more than 2 times that of Case 1 (1.97 m s^{-1}) and Case 2 (2.03 m s^{-1}). As such, case 3 had a superior diffusion condition for pollutants. The crucial weather patterns and the record of rainfall of the three cases are presented in Fig. S2 and Table S1. In Case 1, (typically on 3 September; Fig. S2a), the isobar density of the surface was sparse, accompanied by low wind speed, cloudy weather, and high RH. The diffusion condition was negative in Case 1. In Case 2 (typically on 7 September; Fig. S2b), the sparse isobars on the surface were unfavourable to the diffusion of

Table 1

Concentration ($\mu\text{g m}^{-3}$) of PM_{2.5} and its major species, and the mean values of meteorological parameters.

	September 1–20	Case 1	Case 2	Case 3
PM _{2.5}	23.56	37.48	29.84	14.24
PM ₁₀	34.14	49.49	40.17	26.55
O ₃	100.01	134.09	117.84	72.34
CO	574.06	679.71	677.68	467.29
SO ₂	11.28	11.28	12.75	10.94
NO ₂	16.40	14.16	22.88	12.28
BC ^a	1.04	1.45	1.39	0.51
WSII	18.46	26.27	25.71	9.72
SO ₄ ²⁻	10.40	16.35	13.96	4.99
NO ₃ ⁻	2.81	2.49	4.61	1.80
NH ₄ ⁺	4.37	6.58	6.41	1.88
Na ⁺	0.36	0.26	0.23	0.56
K ⁺	0.23	0.42	0.26	0.15
Mg ²⁺	0.07	0.02	0.02	0.16
Ca ²⁺	0.21	0.15	0.22	0.17
SIA/PM _{2.5}	70.57%	68.30%	79.32%	59.88%
NO ₃ ⁻ /SO ₄ ²⁻	0.35	0.16	0.39	0.47
T	25.14 °C	26.36 °C	25.15 °C	24.62 °C
RH	86.72%	79.14%	86.88%	88.98%
P	100.62 kPa	100.13 kPa	100.62 kPa	100.62 kPa
WS	3.14 m/s	1.97 m/s	2.03 m/s	5.23 m/s

^a The data for BC during 19–20 September was not successfully acquired due to instrument problems.

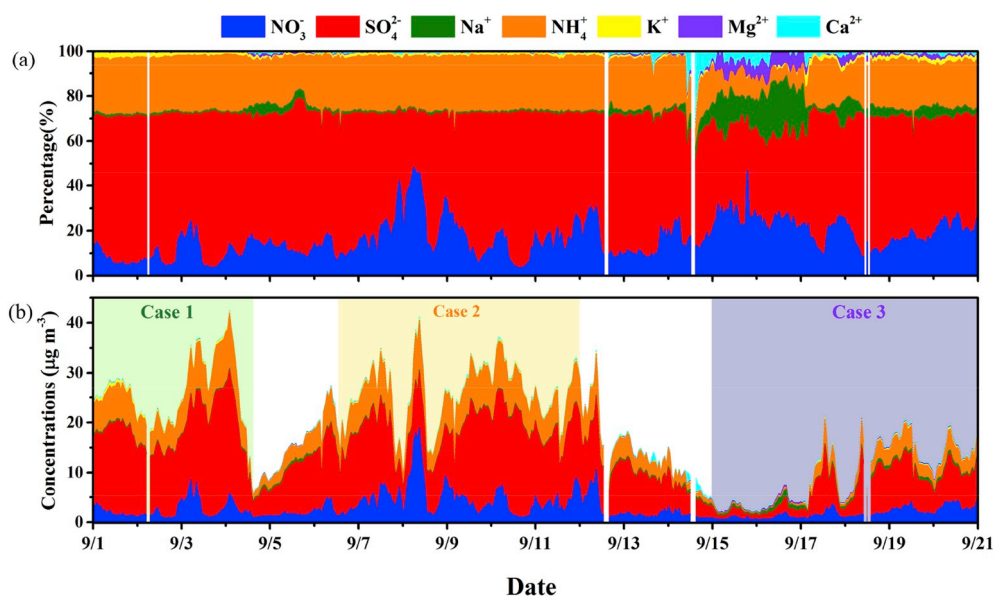


Fig. 3. Mass fraction (a) of each ion in the total water-soluble inorganic ions (WSII) and the mass concentrations (b) of the ions.

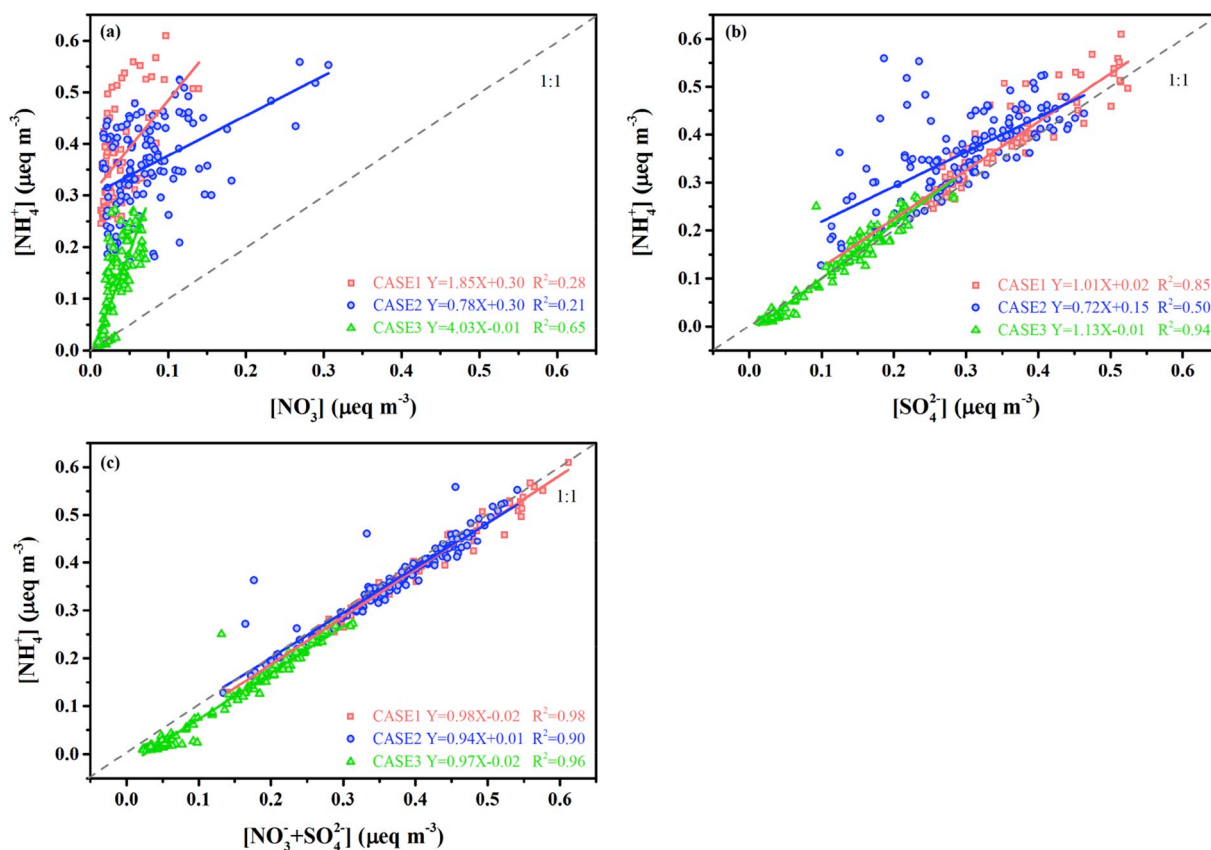


Fig. 4. Pearson correlations between (a) NH_4^+ and NO_3^- , (b) NH_4^+ and SO_4^{2-} , and (c) NH_4^+ and $\text{SO}_4^{2-} + \text{NO}_3^-$.

pollutants. In addition, the transfer of water vapor in the middle level of the atmosphere and the weak surface pressure field could promote the formation of secondary pollutants. In Case 3 (typically on 16–17 September; Figs. S2c and S2d), the southeast wind at 850 hPa and the rainfall at 500 hPa during 15–16 September was caused by the typhoon, which resulted in an improvement of the good air quality. The prevailing winds during 17–20 September at 850 hPa and the surface were the northeast winds and the RH was high. Furthermore, affected by the

strong cold air and the typhoon, the air masses on 17 September came from the north of Ningbo, which could bring some pollutants. Three wet deposition events happened during the typhoon case, one during 15–16 September with extremely large rain capacity of 266.3 mm, and the other two rainfall during 16–18 September with 8.7 mm and 7.3 mm rainfall (Table S1). Overall, the high frequency of rainfall in Case 3 was one of the major reasons for the lower $\text{PM}_{2.5}$ and BC concentrations.

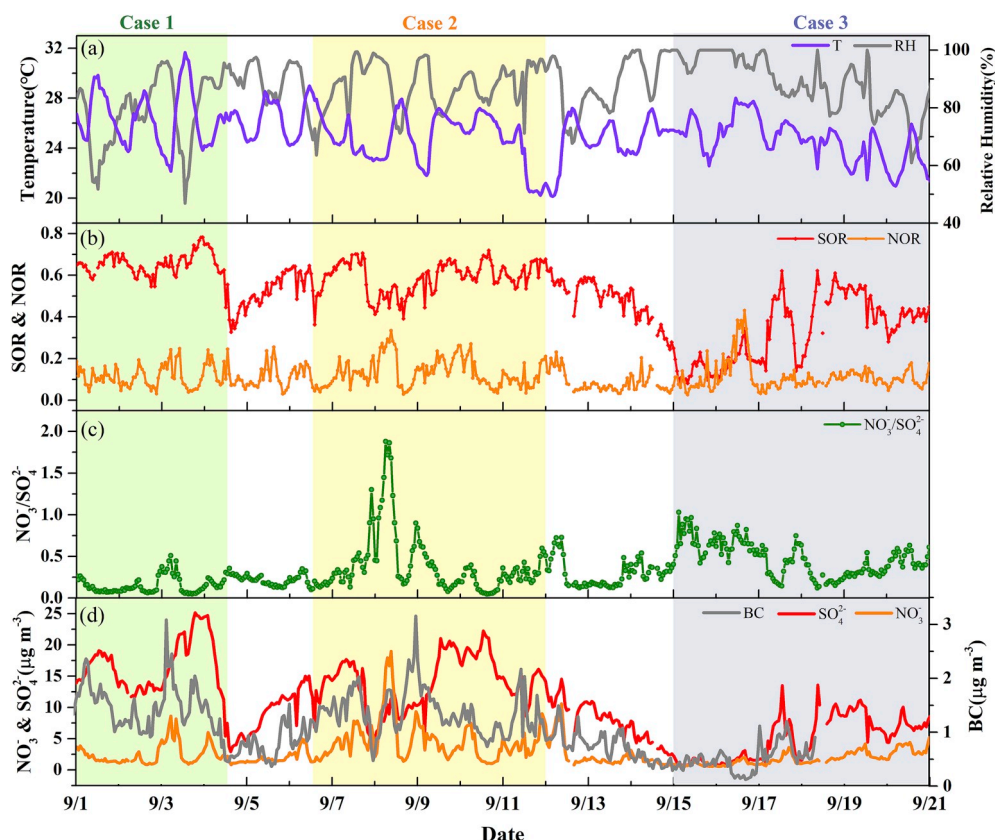


Fig. 5. Time series of temperature and relative humidity (a), SOR and NOR (b), the ratio of $\text{NO}_3^-/\text{SO}_4^{2-}$ (c), SO_4^{2-} , NO_3^- , and BC(d).

3.3. Water-soluble inorganic components of $\text{PM}_{2.5}$

The mean concentration of the total WSII was $18.5 \mu\text{g m}^{-3}$ with a value of 74.0% in $\text{PM}_{2.5}$. The mean concentrations of SO_4^{2-} , NO_3^- , and NH_4^+ (collectively known as the secondary inorganic aerosol, SIA) were $10.4 \mu\text{g m}^{-3}$, $2.8 \mu\text{g m}^{-3}$, $4.4 \mu\text{g m}^{-3}$, respectively. Sulphate was the most abundant species with a proportion of 54.3% of total WSII, followed by ammonium (21.6%) and nitrate (16.3%) during the entire study period. Sulphate, nitrate, and ammonium (SNA) were the major components of WSII with a total of $(92.1 \pm 8.4)\%$, which was in accordance with the results obtained by Hangzhou (Liu et al., 2015), Yangzhou (Ge et al., 2017), Lin'an (Zhang et al., 2017), and the Beijing-Tianjin-Hebei region (Huang et al., 2017).

The time series of the concentration of WSII in $\text{PM}_{2.5}$ and the percentage of each ion in the total WSII are shown in Fig. 3. Specifically, $\text{PM}_{2.5}$ and its major inorganic components presented distinct characteristics in the different cases. The concentration of all WSII except NO_3^- and Ca^{2+} were 0%–61.5% higher in Case 1 than in Case 2. D K^+ yielded the largest increase, indicating a greater impact of biomass burning in Case 1. Differently, the concentration of all WSII distinctly decreased by 22.7%–70.7% except Na^+ and Mg^{2+} in Case 3, compared to Case 2. The mean concentration and fraction of Na^+ and Mg^{2+} increased significantly in Case 3, which confirms the significant impact of maritime air mass due to the typhoon. The Ca^{2+} concentration was slightly lower in Case 1 and Case 3 compared to Case 2, but its proportion was highest in Case 3. This result suggests that the contribution of local construction dust to $\text{PM}_{2.5}$ increased due to the high wind associated with the typhoon.

As tracers of secondary pollution, the mass concentration of SO_4^{2-} was $16.35 \mu\text{g m}^{-3}$ in Case 1 which was 17.1% higher than that in Case 2, and dramatically decreased to $4.99 \mu\text{g m}^{-3}$ in Case 3. The mean mass concentration of NH_4^+ in Case 1 and Case 2 was comparable ($6.6 \mu\text{g m}^{-3}$ versus $6.4 \mu\text{g m}^{-3}$), which were approximately 3 times that of Case 3

($1.9 \mu\text{g m}^{-3}$). The concentration of NO_3^- in Case 1 ($2.5 \mu\text{g m}^{-3}$) and Case 3 ($1.8 \mu\text{g m}^{-3}$) was approximately half that of Case 2 ($4.6 \mu\text{g m}^{-3}$). Fig. S3 depicts the mass fraction of each ion in the total WSII for the different cases. The fraction of SIA in $\text{PM}_{2.5}$ decreased both in Case 1 and Case 3 compared to Case 2. The mass fraction of SO_4^{2-} was always first among the three cases, while the fraction decreased from 62.2% in Case 1–54.4% in Case 2 and 47.3% in Case 3. The proportion of NH_4^+ in WSII was second to SO_4^{2-} in Case 1 (24.9%) and Case 2 (25.0%), but third in Case 3 (16.1%). In comparison, the percentage of NO_3^- in WSII was higher for Case 3 (20.7%) and Case 2 (17.7%), while the percentage was only 9.5% for Case 1. These results show that NO_3^- dominantly accounted for the decreased fraction of SIA in the control case, while SO_4^{2-} and NH_4^+ accounted for the reduction in the typhoon case.

4. Discussions

4.1. Formation mechanism of $\text{PM}_{2.5}$

The three cases occurred under different meteorological conditions and exhibited different chemical characteristics. This study attempted to explore the formation mechanism of $\text{PM}_{2.5}$, particularly, with regard to the secondary inorganic components, with respect to the distinct meteorological conditions of the three cases.

4.1.1. Formation mechanisms of SIA

To better understand the existing form and formation mechanisms of SO_4^{2-} , NO_3^- , and NH_4^+ in the three cases, Pearson correlation analysis of their equivalent concentrations was performed. The equivalent ratio of NH_4^+ to the sum of NO_3^- and SO_4^{2-} was close to 1 (Fig. 4c), indicating the neutralization of sulphate and nitrate by ammonium was almost complete. SO_4^{2-} and NH_4^+ were well-correlated in Case 1 and Case 3 with a high correlation coefficient ($R^2 = 0.85$ and 0.94) (Fig. 4b). For NH_4HSO_4 and $(\text{NH}_4)_2\text{SO}_4$, the equivalent ratio of NH_4^+ and SO_4^{2-} were 0.5 and 1.00,

respectively (Wang et al., 2005b). The line fit of NH_4^+ and SO_4^{2-} revealed a slope of 1.01 for Case 1 and 1.13 for Case 3 (Fig. 4b), suggesting a dominant form of $(\text{NH}_4)_2\text{SO}_4$ over NH_4HSO_4 in both the control case and typhoon case. Previous studies have determined that NO_3^- can also exist as $\text{Ca}(\text{NO}_3)_2$, NaNO_3 , and $\text{Mg}(\text{NO}_3)_2$ (Wang et al., 2006; Gard et al., 1998; Zhang et al., 2015; Hua et al., 2014). Therefore, NO_3^- is poorly correlated with NH_4^+ in the control case ($R^2 = 0.28$) and this may be ascribed to existential forms other than NH_4NO_3 in the atmosphere. Whereas in the typhoon case, a close correlation between NO_3^- and NH_4^+ ($R^2 = 0.65$) suggests that the main existential form is NH_4NO_3 .

4.1.2. Formation mechanism of $\text{PM}_{2.5}$ in case 1

Case 1 occurred under the influence of the control measures. Although the control measures reduced the emission of some pollutants to the atmosphere, the mass concentration of $\text{PM}_{2.5}$ ($37.5 \mu\text{g m}^{-3}$) still exceeded the value ($29.8 \mu\text{g m}^{-3}$) in Case 2 without the control. High SO_4^{2-} but low NO_3^- in Case 1 with respect to Case 2 (in terms of the mass concentration and fraction) could be partially ascribed to the precursors. NO_2 in Case 1 was clearly reduced due to traffic restriction but SO_2 remained at a high level compared to Case 2 (Table 1). The time variation of SOR and NOR is shown in Fig. 5. It should be noted that SOR (0.33–0.78, mean: 0.65) in Case 1 was the highest among the three cases, indicating a high oxidation rate of SO_2 and the importance of photochemical oxidation in the formation of SO_4^{2-} . In addition, the meteorological condition in Case 1 was stagnant and cloudy with high RH (sect. 3.3), which would be favourable for the hygroscopic growth of $\text{PM}_{2.5}$ and the secondary formation of pollutants, especially SO_4^{2-} (Wu et al., 2018). SO_4^{2-} in Case 1 was completely neutralized by NH_4^+ to form $(\text{NH}_4)_2\text{SO}_4$. Specifically, a peak ($25.15 \mu\text{g m}^{-3}$) of SO_4^{2-} in Case 1 occurred during 3–4 September. Some researchers have determined that the existence of NO_2 and NO_3^- is beneficial to the oxidation of SO_2 to SO_4^{2-} (Huang et al., 2014; Xie et al., 2015; Wang et al., 2016). Based on photochemical considerations, O_x ($\text{NO}_2 + \text{O}_3$) presents the total oxidants (Liu et al., 1987). It was observed that the correlation coefficient of SO_4^{2-} with O_x ($R^2 = 0.40$) was higher than that of O_3 ($R^2 = 0.34$) during the entire study period (Fig. S4). The correlation was reinforced when the RH was higher than 85% ($R^2 = 0.50$), while it was not when RH was lower than 85% ($R^2 = 0.21$). These results suggest a stronger promoting effect of NO_2 in the oxidation formation of SO_4^{2-} under a high RH. As shown in Fig. 5, SO_4^{2-} began to increase at 0:00 3 September after the pre-increase of NO_3^- and NO_2 during the night of 2 September. Meanwhile, RH peaked (96%) at 0:00 3 September, which provides an ideal environment for the transformation of SO_2 to SO_4^{2-} , accelerated by NO_2 and NO_3^- .

Despite the low concentration and proportion of NO_3^- in Case 1, an obvious increase of NO_3^- occurred during 2–4 September with a peak value of $8.65 \mu\text{g m}^{-3}$. With respect to the precursor, NO_2 was relatively low during Case 1, with a small increase from 2 to 4 September. It was reported that the low T and high RH condition would promote the heterogeneous reaction of NO_2 to NO_3^- (Wang et al., 2006; Pan et al., 2016). As presented in Fig. 5, the increasing NO_3^- (20:00 2 September – 8:00 3 September) was accompanied with a high RH and low T, which was conducive to the heterogeneous formation of NO_3^- , probably due to the hydrolysis of N_2O_5 given that N_2O_5 plays an important role at night (Zhang et al., 2015). Previous studies have reported that a nitrate could form on a particle's surface via the oxidation of NO_2 , existing as NaNO_3 , NH_4NO_3 , KNO_3 , $\text{Mg}(\text{NO}_3)_2$, and $\text{Ca}(\text{NO}_3)_2$ (Min et al., 2008; Rodhe et al., 2010; Sullivan et al., 2009; Wang et al., 2015; Jia et al., 2003; Gard et al., 1998). Therefore, correlation analysis of NO_3^- and NOR with Na^+ , NH_4^+ , K^+ , Mg^{2+} , and Ca^{2+} was conducted to further investigate the formation mechanism of NO_3^- (Fig. 6). The closer correlation of NOR with NH_4^+ , K^+ , and Ca^{2+} during the morning of 3 September was indicative of the promoting effect of ammonium, biomass, and dust particles in the heterogeneous reaction of NO_2 . The correlation of NO_3^- with NH_4^+ , K^+ , and Ca^{2+} increased during the morning of 3 September. In particular, the correlation of NO_3^- with K^+ over NH_4^+ is indicative of the dominant form

of KNO_3 , which was probably related to the accumulation of biomass particles under the stagnant weather. BC can also be contributed by biomass burning (Schleicher et al., 2013), the highest concentration of NO_3^- on 3 September accompanying with the highest concentration ($3.09 \mu\text{g m}^{-3}$) of BC (Fig. 5).

4.1.3. Formation mechanism of $\text{PM}_{2.5}$ in case 2

Case 2 occurred without control measures, while the meteorological condition was still averse to the diffusion of the pollutants. SO_2 especially NO_2 , exhibited an obvious increase in Case 2 when the control measures ceased. Nonetheless, the concentration of $\text{PM}_{2.5}$ decreased compared to the control period, which was due to the prevailing marine air masses in Case 2. The contribution of SIA to $\text{PM}_{2.5}$ in Case 1 was the highest among the three cases. Both the mass concentration and fraction of NO_3^- in Case 2 were approximately twice that of Case 1. The ratio of $\text{NO}_3^-/\text{SO}_4^{2-}$ in Case 2 was more than twice that of Case 1. This is indicative of the increase of the contribution of mobile sources and the formation process of NO_3^- in pollution (Han et al., 2016a; Huang et al., 2017). As depicted in Fig. 5, NOR was higher in Case 2 than in Case 1 considering the entire case, suggesting a higher oxidation efficiency of NO_2 in the formation of NO_3^- . In addition to the chemical factor, the meteorological condition was stagnant and had a higher RH that was beneficial for the formation of NO_3^- . Therefore, a higher gaseous precursor and high RH condition could explain the significant increase of the contribution of NO_3^- in Case 2.

Noticeably, rapid growth of NO_3^- occurred in the morning (0:00–10:00) of 8 September and reached its peak value ($18.98 \mu\text{g m}^{-3}$) of the observation period. In addition, NO_2 as well as NOR, had a significant increase that morning, which represents high NO_2 during the high transformation reaction. A stronger correlation existed between either Na^+ , K^+ , and Ca^{2+} with NOR in the morning of 8 September compared to the entire Case 2 (Fig. 6), indicating the strengthening of the heterogeneous formation of NO_3^- on the surface of sea salt, biomass burning particles, and dust. Simultaneously, the mass concentration of BC also had rapid growth in the morning of 8 September, which might be contributed by biomass burning. The precipitation resulted in a high RH and low T (Fig. 5a) in the morning of 8 September and could lead to the heterogeneous formation of NO_3^- . Moreover, NO_3^- had a stronger correlation with NH_4^+ , Na^+ , K^+ , Ca^{2+} , suggesting that NH_4NO_3 , NaNO_3 , KNO_3 , $\text{Ca}(\text{NO}_3)_2$ were the forms of nitrate in the morning of 8 September. Thus, a significant increase of NO_2 from the mobile source mainly accounted for the high concentration of NO_3^- in Case 2. The occasionally rapid growth of NO_3^- was caused by the heterogeneous reactions of NO_2 on the surface of sea salt, biomass particles, and dust particles.

4.1.4. Formation mechanism of $\text{PM}_{2.5}$ in case 3

Case 3 was characterized by the influence of the typhoon. The $\text{PM}_{2.5}$ concentration ($14.24 \mu\text{g m}^{-3}$) and most of its water-soluble inorganic chemical components were a minimum in Case 3 (Table 1). The mass concentrations and proportions of marine tracers (Na^+ and Mg^{2+}) increased substantially in Case 3 (Fig. 3), which might be due to the sea wind and marine air masses introduced by the typhoon. There are two distinct stages in the typhoon case. During the early stage (15–16 September) when the typhoon was on the sea surface in the southeast of the observation site, $\text{PM}_{2.5}$ was extremely low due to the influence of sea wind. Whereas, the concentration and proportion of Na^+ and Mg^{2+} were the highest during the entire observation period. The contribution of NO_3^- to WSII clearly increased, while the proportion of SO_4^{2-} decreased. After 16 September, the wind direction changed to northwest from southeast although the wind speed remained high, which could have introduced pollutants from the north of Ningbo. The increase of SO_4^{2-} was the major driving factor for the increase of $\text{PM}_{2.5}$ during 17–20 September. The increase of SO_2 was more obvious from 16 September, which provided enough precursors for the formation of sulphates. This result was supported by the increasing level of SOR from 17 to 20

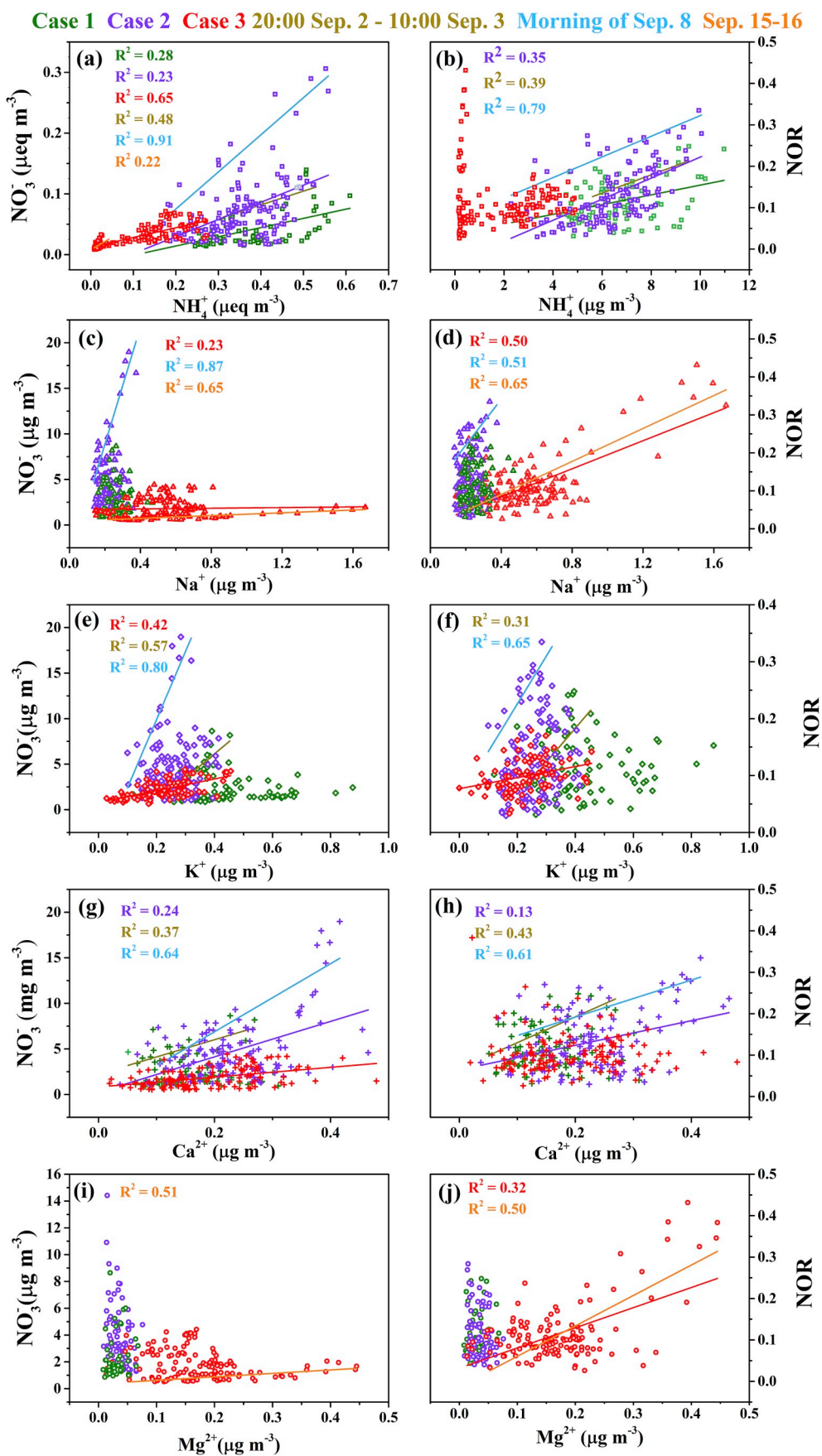


Fig. 6. Correlation analysis between NO_3^- and NOR with (a, b) NH_4^+ , (c, d) Na^+ , (e, f) K^+ , (g, h) Ca^{2+} , and (i, j) Mg^{2+} .

September.

From the entire Case 3, SIA was still the most abundant components in PM_{2.5}. SO₂ and NO₂ were comparable in the typhoon case with the control case. The mass fraction of NO₃⁻ was highest in Case 3, while the mass fraction of SO₄²⁻ was lowest on the contrary. NOR was well correlated with Na⁺ and Mg²⁺, suggesting the promoting effect of sea salt on the oxidation of NO₂ for the entire case. The major forms of nitrates were NH₄NO₃ and KNO₃ given that NO₃⁻ was better correlated with NH₄⁺ and K⁺ than with other cations in Case 3. During the early stage of the typhoon, the precursors, i.e., SO₂ and NO₂ both decreased by a large margin, whereas SOR and NOR were elevated during this stage. In particular, the highest NOR of the entire observation period occurred, which is indicative of the high transformation reaction of NO₂. From Fig. 6, the close correlation of NOR with Na⁺ and Mg²⁺ was determined. This indicated the promoting effect of sea salt on the oxidation of NO₂. RH was maintained at the high level of >90% during 15–16 September, which offers beneficial condition for the heterogeneous reaction of NO₂ on the surface of sea salt to form nitrates. The correlation of NO₃⁻ with Na⁺ and Mg²⁺ exceeded the correlation with NH₄⁺ during 15–16 September. This result suggests that the nitrates were mainly in the form of NaNO₃ and Mg(NO₃)₂ instead of NH₄NO₃, with the sudden interference of the typhoon. Therefore, the heterogeneous reaction of NO₂ on the substantial sea salt under moist condition could explain the high contribution of NO₃⁻ to PM_{2.5} during the early stage of the typhoon.

5. Conclusions

In this study, we characterized the water-soluble inorganic chemical components and BC of PM_{2.5} and discussed the formation of SIA with the influence of the strict control measures and a typhoon in Ningbo during September 2016. The mean concentrations of PM_{2.5} were 37.48, 29.84, and 14.24 μg m⁻³ in the control case, normal case, and typhoon case, respectively. The effect of mitigation measures on PM_{2.5} concentration was far offset by the influence of stable weather and regional transport in the control case. SIA was the dominant composition with decreasing contribution from the normal case (79.3%) to the control case (68.3%) and the typhoon case (59.9%). The typhoon weather and mitigation measures both slightly decrease the SO₂ and remarkably decrease the NO₂. However, the contribution of SO₄²⁻ to PM_{2.5} in the control case has little increase compared to that in the normal case. While as for the typhoon case, similar situation occurred for NO₃⁻. The formation of SO₄²⁻ was most active in the control case for its high SOR. Moreover, NO₃⁻ and NO₂ in the high RH condition (>85%) promoted the occasionally rapid growth of SO₄²⁻. Therefore, the high RH and pre-increase of NO₃⁻ and NO₂ lead to the active formation of SO₄²⁻ in the control case by photochemical reaction. Twice rapid increase of nitrate in the control and normal cases were accompanied with the quickly increase of BC and strong correlation between K⁺ and NOR, which suggested the influence of biomass burning on the formation of NO₃⁻. Strong correlation of Na⁺ and Mg²⁺ with NOR was found in the Typhoon case. Sea salt brought by the typhoon provided a surface for the heterogeneous formation of NO₃⁻, which was diagnosed as the main cause of the formation of NO₃⁻ in the typhoon case even under the low NO₂ condition. Our results suggest that the strict control measures during the G20 summit had positive effect on reducing the PM_{2.5}. However, the effect may be offset by the accumulation of gaseous precursors and secondary formation, which need more attention when implemented the mitigation measures.

Declaration of competing interest

The authors declare that they have no known competing financial interests or personal relationships that could have appeared to influence the work reported in this paper.

CRedit authorship contribution statement

Yanru Zhang: Conceptualization, Methodology, Software, Investigation, Writing - review & editing. **Zhenyu Hong:** Methodology, Software, Writing - original draft. **Jinsheng Chen:** Conceptualization, Supervision, Writing - review & editing. **Lingling Xu:** Conceptualization, Writing - review & editing. **Youwei Hong:** Writing - original draft. **Mengren Li:** Writing - original draft. **Hongfei Hao:** Investigation, Writing - original draft. **Yanting Chen:** Investigation. **Yuqing Qiu:** Investigation. **Xin Wu:** Investigation. **Jian-Rong Li:** Data curation. **Lei Tong:** Data curation. **Hang Xiao:** Data curation.

Acknowledgements

This study was funded by the National Key Research and Development Program (2016YFC02005 & 2016YFE0112200), the National Natural Science Foundation of China (41575146), the Chinese Academy of Sciences Interdisciplinary Innovation Team Project, and the Natural Science Foundation of Fujian Province, China (2016J01201).

Appendix A. Supplementary data

Supplementary data to this article can be found online at <https://doi.org/10.1016/j.atmosenv.2020.117312>.

References

- Cowen, K., Hanft, E., Kelly, T., Dindal, A., McKernan, J., 2012-11-5. Environmental Technology Verification Report: ETV Advanced Monitoring Systems Center Applikon MARGA Semi-continuous Ambient Air Monitoring System. Battelle and US Environmental Protection Agency. <http://nepis.epa.gov/Exec/zyPDF.cgi,2011>.
- Draxler, R.R., Hess, G.D., Draxler, R.R., 1997. Description OF the HYSPLIT_4 modeling system. Nat. Ocean. Atmos. Adm. Tech. Memorand. Erl Arl 197-199.
- Fang, G.C., Lin, S.J., Chang, S.Y., Chou, C.C.K., 2009. Effect of typhoon on atmospheric particulates in autumn in central Taiwan. Atmos. Environ. 43, 6039-6048.
- Fu, Q., Zhuang, G., Wang, J., Xu, C., Huang, K., Li, J., Hou, B., Lu, T., Streets, D.G., 2008. Mechanism of formation of the heaviest pollution episode ever recorded in the Yangtze River Delta, China. Atmos. Environ. 42, 2023-2036. <https://doi.org/10.1016/j.atmosenv.2007.12.002>.
- Gard, E.E., Kleeman, M.J., Gross, D.S., Hughes, L.S., Allen, J.O., Morrical, B.D., Ferguson, D.P., Dienes, T., Gälli, M.E., Johnson, R.J., 1998. Direct observation of heterogeneous chemistry in the atmosphere. Science 279, 1184-1187.
- Ge, X., Li, L., Chen, Y., Chen, H., Wu, D., Wang, J., Xie, X., Ge, S., Ye, Z., Xu, J., Chen, M., 2017. Aerosol characteristics and sources in Yangzhou, China resolved by offline aerosol mass spectrometry and other techniques. Environ. Pollut. 225, 74-85. <https://doi.org/10.1016/j.envpol.2017.03.044>.
- George, C., Ammann, M., D'Anna, B., Donaldson, D.J., Nizkorodov, S.A., 2015. Heterogeneous photochemistry in the atmosphere. Chem. Rev. 115, 4218.
- Han, B., Zhang, R., Yang, W., Bai, Z.P., Ma, Z.Q., Zhang, W.J., 2016a. Heavy haze episodes in Beijing during January 2013: inorganic ion chemistry and source analysis using highly time-resolved measurements from an urban site. Sci. Total Environ. 544, 319-329.
- Han, X., Guo, Q., Liu, C., Strauss, H., Yang, J., Hu, J., Wei, R., Tian, L., Kong, J., Peters, M., 2016b. Effect of the pollution control measures on PM_{2.5} during the 2015 China Victory Day Parade: implication from water-soluble ions and sulfur isotope. Environ. Pollut. 218, 230-241. <https://doi.org/10.1016/j.envpol.2016.06.038>.
- Hua, W., Verreault, D., Allen, H.C., 2014. Surface electric fields of aqueous solutions of NH₄NO₃, Mg(NO₃)₂, NaNO₃, and LiNO₃: implications for atmospheric aerosol chemistry. J. Phys. Chem. C 118, 24941-24949.
- Hua, Y., Wang, S., Wang, J., Jiang, J., Zhang, T., Song, Y., Kang, L., Zhou, W., Cai, R., Wu, D., 2016. Investigating the impact of regional transport on PM_{2.5} formation using vertical observation during APEC 2014 Summit in Beijing. Atmos. Chem. Phys. 16, 15451-15460.
- Huang, K., Zhuang, G., Lin, Y., Fu, J.S., Wang, Q., Liu, T., Zhang, R., Jiang, Y., Deng, C., Fu, Q., Hsu, N.C., Cao, B., 2012. Typical types and formation mechanisms of haze in an Eastern Asia megacity, Shanghai. Atmos. Chem. Phys. 12, 105-124. <https://doi.org/10.5194/acp-12-105-2012>.
- Huang, X., Song, Y., Zhao, C., Li, M., Zhu, T., Zhang, Q., Zhang, X., 2014. Pathways of sulfate enhancement by natural and anthropogenic mineral aerosols in China. J. Geophys. Res. Atmos. 119 (719), 735-753.
- Huang, X., Liu, Z., Liu, J., Hu, B., Wen, T., Tang, G., Zhang, J., Wu, F., Ji, D., Wang, L., Wang, Y., 2017. Chemical characterization and source identification of PM_{2.5} at multiple sites in the Beijing-Tianjin-Hebei region, China. Atmos. Chem. Phys. 17, 12941-12962. <https://doi.org/10.5194/acp-17-12941-2017>.
- Jia, L., Posfai, M., Hobbs, P.V., Buseck, P.R., 2003. Individual aerosol particles from biomass burning in southern Africa compositions and aging of inorganic particles. J. Geophys. Res. 108.

- Li, X., Wang, L., Wang, Y., Wen, T., Yang, Y., Zhao, Y., Wang, Y., 2012. Chemical composition and size distribution of airborne particulate matters in Beijing during the 2008 Olympics. *Atmos. Environ.* 50, 278–286. <https://doi.org/10.1016/j.atmosenv.2011.12.021>.
- Li, P., Yan, R., Yu, S., Wang, S., Liu, W., Bao, H., 2015. Reinstate regional transport of PM_{2.5} as a major cause of severe haze in Beijing. *Proc. Natl. Acad. Sci. Unit. States Am.* 112, E2739–E2740.
- Li, G., Bei, N., Cao, J., Huang, R., Wu, J., Feng, T., Wang, Y., Liu, S., Zhang, Q., Tie, X., 2017a. A possible pathway for rapid growth of sulfate during haze days in China. *Atmos. Chem. Phys.* 17, 1–43.
- Li, H., Ma, Y., Duan, F., He, K., Zhu, L., Huang, T., Kimoto, T., Ma, X., Ma, T., Xu, L., 2017b. Typical winter haze pollution in Zibo, an industrial city in China: characteristics, secondary formation, and regional contribution. *Environ. Pollut.* 229, 339–349.
- Li, K., Chen, L., White, S.J., Zheng, X., Lv, B., Lin, C., Bao, Z., Wu, X., Gao, X., Ying, F., Shen, J., Azzi, M., Cen, K., 2017c. Chemical characteristics and sources of PM₁ during the 2016 summer in Hangzhou. *Environ. Pollut.* <https://doi.org/10.1016/j.envpol.2017.09.016>.
- Li, P., Wang, L., Guo, P., Yu, S., Mehmood, K., Wang, S., Liu, W., Seinfeld, J.H., Zhang, Y., Wong, D.C., 2017d. High reduction of ozone and particulate matter during the 2016 G-20 summit in Hangzhou by forced emission controls of industry and traffic. *Environ. Chem. Lett.* 15, 709–715.
- Liang, P., Zhu, T., Fang, Y., Li, Y., Han, Y., Wu, Y., Hu, M., Wang, J., 2017. The role of meteorological conditions and pollution control strategies in reducing air pollution in Beijing during APEC 2014 and parade 2015. *Atmos. Chem. Phys.* 1–62.
- Liu, G., Li, J., Wu, D., Xu, H., 2015. Chemical composition and source apportionment of the ambient PM_{2.5} in Hangzhou, China. *Particology* 18, 135–143. <https://doi.org/10.1016/j.partic.2014.03.011>.
- Liu, S.C., Fehsenfeld, F.C., Parrish, D.D., Williams, E.J., Fahey, D.W., Hübler, G., Murphy, P.C., 1987. Ozone production in the rural troposphere and the implications for regional and global ozone distribution. *J. Geophys. Res. Atmos.* 92, 4191–4207.
- Min, H., Slanina, Z.W., Peng, L., Shang, L., Zeng, L., 2008. Acidic gases, ammonia and water-soluble ions in PM_{2.5} at a coastal site in the Pearl River Delta, China. *Atmos. Environ.* 42, 6310–6320.
- Ming, L., Jin, L., Li, J., Fu, P., Yang, W., Liu, D., Zhang, G., Wang, Z., Li, X., 2017. PM_{2.5} in the Yangtze River Delta, China: chemical compositions, seasonal variations, and regional pollution events. *Environ. Pollut.* 223, 200–212. <https://doi.org/10.1016/j.envpol.2017.01.013>.
- Pan, Y., Wang, Y., Zhang, J., Liu, Z., Wang, L., Tian, S., Tang, G., Gao, W., Ji, D., Tao, S., 2016. Redefining the importance of nitrate during haze pollution to help optimize an emission control strategy. *Atmos. Environ.* 141, S135223101630468X.
- Rodhe, H., Crutzen, P., Vanderpol, A., 2010. Formation of sulfuric and nitric acid in the atmosphere during long-range transport. *Tellus* 33, 132–141.
- Schleicher, N., Norra, S., Dietze, V., Yu, Y., Fricker, M., Kaminski, U., Chen, Y., Cen, K., 2011. The effect of mitigation measures on size distributed mass concentrations of atmospheric particles and black carbon concentrations during the Olympic Summer Games 2008 in Beijing. *Sci. Total Environ.* 412, 185–193.
- Schleicher, N., Norra, S., Chen, Y., Chai, F., Wang, S., 2012. Efficiency of mitigation measures to reduce particulate air pollution—a case study during the Olympic Summer Games 2008 in Beijing, China. *Sci. Total Environ.* 427–428, 146–158. <https://doi.org/10.1016/j.scitotenv.2012.04.004>.
- Schleicher, Nina, Norra, Stefan, Fricker, Mathieu, Kaminski, Uwe, Chen, Yizhen, Chai, Fahe, Wang, Shulan, Yang, Yu, Kuang, Cen, 2013. Spatio-temporal variations of black carbon concentrations in the Megacity Beijing. *Environ. Pollut.* 182, 392–401.
- Stein, A.F., Draxler, R.R., Rolph, G.D., Stunder, B.J.B., Cohen, M.D., Ngan, F., 2016. NOAA's HYSPLIT atmospheric transport and dispersion modeling system. *Bull. Am. Meteorol. Soc.* 96 (150504130527006).
- Sullivan, R.C., Moore, M.J.K., Petters, M.D., Kreidenweis, S.M., Roberts, G.C., Prather, K.A., 2009. Effect of chemical mixing state on the hygroscopicity and cloud nucleation properties of calcium mineral dust particles. *Atmos. Chem. Phys.* 9, 3303–3316. <https://doi.org/10.5194/acp-9-3303-2009>.
- Sun, Y., Zhuang, G., Tang, A.A., Wang, Y., An, Z., 2006. Chemical characteristics of PM_{2.5} and PM₁₀ in haze-fog episodes in Beijing. *Environ. Sci. Technol.* 40, 3148–3155.
- Sun, Y., Wang, L., Wang, Y., Quan, L., Zirui, L., 2011. In situ measurements of SO₂, NO_x, NO_y, and O₃ in Beijing, China during August 2008. *Sci. Total Environ.* 409, 933–940.
- Sun, Y., Wang, Z., Wild, O., Xu, W., Chen, C., Fu, P., Wei, D., Zhou, L., Zhang, Q., Han, T., 2016. "APEC Blue": secondary aerosol reductions from emission controls in Beijing. *Sci. Rep.* 6, 20668.
- Wang, G., Cheng, C., Meng, J., Huang, Y., Li, J., Ren, Y., 2015. Field observation on secondary organic aerosols during Asian dust storm periods: formation mechanism of oxalic acid and related compounds on dust surface. *Atmos. Environ.* 113, 169–176.
- Wang, G., Zhang, R., Gomez, M.E., Yang, L., Zamora, M.L., Hu, M., Lin, Y., Peng, J., Guo, S., Meng, J., 2016. Persistent sulfate formation from London Fog to Chinese haze. *Proc. Natl. Acad. Sci. U. S. A.* 113, 13630.
- Wang, H., Tian, M., Chen, Y., Shi, G., Cao, X., 2018. Seasonal characteristics, formation mechanisms and source origins of PM_{2.5} in two megacities in Sichuan Basin, China. *Atmos. Chem. Phys.* 18, 865–881.
- Wang, T., Nie, W., Gao, J., Xue, L.K., 2010. Air quality during the 2008 Beijing Olympics: secondary pollutants and regional impact. *Atmos. Chem. Phys.* 10, 7603–7615.
- Wang, Y., Zhuang, G., Sun, Y., An, Z., 2005a. Water-soluble part of the aerosol in the dust storm season—evidence of the mixing between mineral and pollution aerosols. *Atmos. Environ.* 39, 7020–7029.
- Wang, Y., Zhuang, G., Tang, A., Yuan, H., Sun, Y., Chen, S., Zheng, A., 2005b. The ion chemistry and the source of PM_{2.5} aerosol in Beijing. *Atmos. Environ.* 39, 3771–3784.
- Wang, Y., Zhuang, G., Zhang, X., Huang, K., Xu, C., Tang, A., Chen, J., An, Z., 2006. The ion chemistry, seasonal cycle, and sources of PM_{2.5} and TSP aerosol in Shanghai. *Atmos. Environ.* 40, 2935–2952.
- Wu, Z., Yu, W., Tan, T., Zhu, Y., Zhang, Y., 2018. Aerosol liquid water driven by anthropogenic inorganic salts: implying its key role in the haze formation over north China plain. *Environ. Sci. Technol. Lett. acs. estlett.* 8b00021.
- Xie, Y., Ding, A., Nie, W., Mao, H., Qi, X., Huang, X., Xu, Z., Kerminen, V.M., Petäjä, T., Chi, X., 2015. Enhanced sulfate formation by nitrogen dioxide: implications in situ observations at the SORPES station. *J. Geophys. Res. Atmos.* 120 n/a-n/a.
- Xu, W., Song, W., Zhang, Y., Liu, X., Zhang, L., Zhao, Y., Liu, D., Tang, A., Yang, D., Wang, D., 2017. Air quality improvement in a megacity: implications from 2015 Beijing Parade Blue pollution control actions. *Atmos. Chem. Phys.* 17, 1–45.
- Yan, J., Chen, L., Lin, Q., Zhao, S., Zhang, M., 2016. Effect of typhoon on atmospheric aerosol particle pollutants accumulation over Xiamen, China. *Chemosphere* 159, 244–255.
- Zhang, R., Wang, G., Guo, S., Zamora, M.L., Ying, Q., Lin, Y., Wang, W., Hu, M., Wang, Y., 2015. formation of urban fine particulate matter. *Chem. Rev.* 115, 3803.
- Zhang, Y., Zhang, H., Deng, J., Du, W., Hong, Y., Xu, L., Qiu, Y., Hong, Z., Wu, X., Ma, Q., Yao, J., Chen, J., 2017. Source regions and transport pathways of PM_{2.5} at a regional background site in East China. *Atmos. Environ.* 167, 202–211. <https://doi.org/10.1016/j.atmosenv.2017.08.031>.